Tong, S. S., Lowe, M. C., Truth, M. A., Minmaugh, E. G., Ginsburg, E., Hirokata, Y., & Gram, T. E. (1982) *Exp. Mol. Pathol. 37*, 358-369.
Towbin, S. A., Strachelin, T., & Gorden, J. (1979) *Proc. Natl. Acad. Sci. U.S.A. 84*, 4761-4771.
Uno, T., Yokota, H., & Imai, Y. (1990) *Biochem. Biophys. Res. Commun. 167*, 498-503.
Van Bladeren, P. J., Vyas, K. P., Sayer, J. M., Ryan, D. E., Thomas, P. E., Levin, W., & Jerina, D. M. (1984) *J. Biol. Chem. 259*, 8966-8973.
Warren, D. L., Brown, D. L., Jr., & Buckpitt, A. R. (1982) *Chem.-Biol. Interact. 40*, 287-303.

Electron Spin Echo Envelope Modulation Studies of the Cu(II)-Substituted Derivative of Isopenicillin N Synthase: A Structural and Spectroscopic Model†

Feng Jiang* and Jack Peisach
Department of Molecular Pharmacology, Albert Einstein College of Medicine of Yeshiva University, Bronx, New York 10461
Li-June Ming and Lawrence Que, Jr.
Department of Chemistry, University of Minnesota, Minneapolis, Minnesota 55455
Victor J. Chen
Lilly Research Laboratories, Indianapolis, Indiana 46285
Received May 3, 1991; Revised Manuscript Received August 28, 1991

ABSTRACT: Electron spin echo evelope modulation spectroscopy (ESEEM) was used to study the active site structure of isopenicillin N synthase (IPNS) from *Cephalosporium acremonium* with Cu(II) as a spectroscopic probe. Fourier transform of the stimulated electron spin-echo envelope for the Cu(II)-substituted enzyme, Cu(II)IPNS, revealed two nearly magnetically equivalent, equatorially coordinated His imidazoles. The superhyperfine coupling constant, A_{iso}, for the remote ^{14}N of each imidazole was 1.65 MHz. The binding of substrate to the enzyme altered the magnetic coupling so that A_{iso} is 1.30 MHz for one nitrogen and 2.16 MHz for the other. From a comparison of the ESEEM of Cu(II)IPNS in D_2O and H_2O, it is suggested that water is a ligand of Cu(II) and this is displaced upon the addition of substrate.

Isopenicillin N synthase (IPNS) is a non-heme iron(II)-containing enzyme found in penicillin- and cephalosporin-producing microorganisms (Baldwin & Abraham, 1988; Robinson, 1988; Baldwin, 1989; Chen et al., 1989; Baldwin & Bradley, 1990). This enzyme catalyzes the oxidative ring closure reactions of δ-(L-α-aminoadipoyl)-L-cysteinyl-D-valine (ACV) to form isopenicillin N, the precursor of all other penicillins, with concomitant four-electron reduction of a single equivalent of dioxygen to form 2 equiv of H_2O. The oxidation of ACV to form the β-lactam and thiazolidine rings was found to be catalyzed by IPNS with complete retention of configuration.

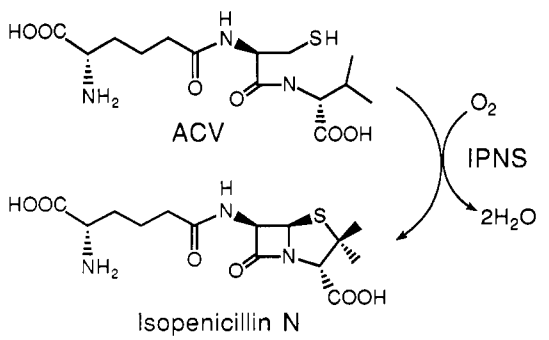

† This work was supported by NIH Grants GM-40168 and RR-02583 to J.P. and GM-33162 to L.Q.
* To whom correspondence should be addressed.

Insights into the mechanism of IPNS catalysis have been obtained from kinetic studies using different substrate analogues (Baldwin, 1989; Baldwin & Abraham, 1988; Robinson, 1988; Baldwin & Bradley, 1990); however, much less has been learned about the active site structure of the enzyme and the configuration of the enzyme–substrate complex. In our previous communication (Ming et al., 1990), we have shown that the Cu(II)-substituted IPNS [Cu(II)IPNS] could be used for spectroscopic studies of the active site structure of the enzyme. A direct interaction of the Cys-S moiety of the substrate with Cu(II) in the active site was clearly demonstrated by an intense S-to-Cu charge-transfer band at 385 nm. Both EPR and electronic spectra of Cu(II)IPNS showed a tetragonally distorted type 2 copper site. The presence of endogenous His residues has also been suggested by NMR studies of Fe(II)-IPNS and Co(II)IPNS.

Pulsed EPR spectroscopy is a powerful technique for the study of the active site structure of copper enzymes (Mims & Peisach, 1981; McCracken et al., 1987; Mims et al., 1984; Zweier et al., 1982). By measuring the electron spin echo envelope modulation (ESEEM) arising from the superhyperfine interaction between Cu(II) and nearby weakly coupled nuclei, we can identify the type and the number of Cu(II) ligands. We report here our ESEEM studies of Cu(II)IPNS which show the presence of two equatorially coordinated His residues and also provide insights into the substrate interaction and solvent accessibility at the active site of this biomedically significant metalloenzyme.

0006-2960/91/0430-11437$02.50/0

Experimental Procedures

Materials and Methods. Isopenicillin N synthase from *Cephalosporium acremonium* (MW 38 400) was isolated as the apo form from recombinant *Escherichia coli* according to reported procedures (Kriauciunas et al., 1991). The substrate ACV was from Incell (Milwaukee, WI), and all other chemicals used were commercially available. The catalytic activity of Fe(II)-reconstituted IPNS was determined from the initial rate of dioxygen consumption with ACV in 0.1 M MOPS, pH 7.1 and 25 °C, and/or by direct measurement by HPLC of the isopenicillin N produced under the above conditions [1 unit of IPNS activity is defined on the basis of consumption (formation) of 1 μmol of O_2 (isopenicillin N)/min under the above conditions]. Those enzyme preparations with specific activity of >4 units/mg when reconstituted with Fe(II) were pooled and concentrated by ultrafiltration and then stored in liquid nitrogen until used.

Cu(II)IPNS was prepared by slow infusion of Cu(II) into apo-IPNS in 0.1 M MOPS buffer at the desired pH. The enzyme samples in D_2O buffer were prepared first by dialyzing the apo-IPNS solution against 0.1 M MOPS in D_2O at pD 7.1 to deuterate solvent-exchangeable protons in the protein, followed by Cu(II) reconstitution. The substrate complex of Cu(II)IPNS was prepared by the addition of ≥1 equiv of ACV to a Cu(II)IPNS solution under anaerobic conditions. The formation of Cu(II)IPNS and the Cu(II)IPNS–ACV complex was monitored by both visible and EPR spectroscopies (Ming et al., 1990).

Spectroscopy and Spectral Simulation. Continuous-wave (CW) EPR spectra were obtained with a Varian E-112 spectrometer, equipped with a Varian NMR gauss meter and a Systron Donner frequency counter. Spectral simulations were carried out by a method described previously (Nilges, 1979; Belford & Nilges, 1979; Maurice, 1981). ESEEM were obtained with a pulsed EPR spectrometer discussed in detail elsewhere (McCracken et al., 1987). It uses a reflection cavity system (Lin et al., 1985), employing a folded stripline cavity (Britt & Klein, 1987), which can accommodate frozen samples in conventional 3 mm i.d., quartz EPR tubes. Multifrequency measurements within the X-band range were achieved by using different resonators. Both two-pulse (90°–τ–180°) and stimulated echo or three-pulse (90°–τ–90°–T–90°) data were collected. The values of τ in a stimulated echo pulse sequence were chosen as a multiple of the periodicity arising from the proton nuclear Zeeman interaction in order to suppress the modulations arising from protons (Mims & Peisach, 1979). ESEEM spectra were obtained by Fourier transform using a modified version of the dead time reconstruction method of Mims (1984).

Simulation of ESEEM spectra were achieved by using the density matrix formalism of Mims (1972), together with an angle-selection averaging scheme for angle-selected ENDOR (Hurst et al., 1985; Henderson et al., 1985). For a randomly oriented sample, as in frozen solution, the molecules can assume any orientation with respect to the external magnetic field, and all contribute to give an anisotropic EPR spectrum. When the ESEEM was performed at a fixed magnetic field, only molecules with certain orientations that experience the same effective magnetic field are selected. For Cu(II)IPNS, like most square-planar copper complexes studied, the ESEEM spectrum at $g_\parallel$ is contributed only by molecules with g_{zz} parallel to the external magnetic field. At X-band, when the anisotropy of the hyperfine interaction is large, there is an overlap between components of $g_\parallel$ and $g_\perp$ and the EPR spectrum shows a "foldover" with the appearance of some $g_\parallel$ features at a higher magnetic field than $g_\perp$ features. In this situation, molecules with many different orientations are selected at the $g_\perp$ setting, and a powder average of many single-crystal spectra is obtained. If the superhyperfine interaction between the Cu(II) unpaired electron and the nucleus of a particular ligand which gives rise to an ESEEM is the same for Cu(II) centers in the sample with different CW EPR parameters, the ESEEM recorded at $g_\perp$ would be the same, regardless of a difference of other ligands (Jiang et al., 1990). The inhomogeneity of the metal binding site, thus, would have very little effect on the ESEEM spectrum.

Nitrogen Modulation. The modulation of ESE is attributed to superhyperfine coupling, arising from the electron–nuclear interactions and the nuclear quadrupole interactions (NQI). The frequencies associated with the ESE envelope modulation function reflect the small splitting of the magnetic energy levels by this superhyperfine interaction. At X-band, the electron–nuclear interaction between the Cu(II) unpaired electron and the remote nitrogen of equatorially bound imidazole is almost as strong as the nuclear Zeeman interaction (Mims & Peisach, 1978), characteristic of the "exact cancellation" condition (Flanagan & Singel, 1987). Therefore, for one of the two ^{14}N manifolds, the two kinds of interactions cancel each other, yielding three sharp "zero-field" nuclear quadrupole resonance lines, whose frequencies, $\nu_\pm$ and ν_0, are almost solely determined by the nuclear quadrupole interaction, so that

$$\nu_\pm = {}^3/_4(e^2qQ)(1 \pm \eta/3)$$

$$\nu_0 = {}^1/_2(e^2qQ)(\eta)$$

The quadrupole coupling constant and the asymmetry parameter, e^2qQ and η, respectively, expressing the magnitude and the symmetry of the quadrupole interaction, therefore, are determined by the frequencies of these NQI lines.

As long as the "exact cancellation" condition is approximately satisfied, the NQI parameters can be determined directly from the frequencies of the three sharp lines. More accurately, they are determined by spectral simulation. For the other spin manifold, the nuclear Zeeman splitting is doubled by the electron–nuclear interaction. One obtains a line representing a $\Delta M_I = 2$ transition at a frequency twice as great as the electron–nuclear coupling. Due to the anisotropy of the electron–nuclear interaction, this line is broadened. The electron–nuclear coupling parameter A_{iso} and the effective distance between the unpaired electron and its interacting nucleus r_{eff}, assuming a point dipole–dipole model, are determined by an overall fitting of the double quantum transition in the ESEEM spectrum at different magnetic fields and different microwave frequencies.

When there is more than a single nitrogen interacting with the unpaired electron, the product of ESE envelope modulation functions of each of them results in the appearance of combinations of the ^{14}N NQI and double quantum lines, whose amplitudes are a measurement of the number of interacting nitrogens (Mims, 1972). The relative intensities of these combination lines as well as the primary NQI lines are determined by the relative orientation of the principal axis of the electric field gradient (efg) tensor of each interacting nitrogen to that of the g tensor (Flanagan & Singel, 1987). But the relative orientation of two principal axis systems (PAS's) and the position of each nitrogen relative to the unpaired electron cannot be uniquely determined in a powder spectrum, because of the complication of the presence of more than a single nitrogen. The Euler angles between two PAS's and the spherical polar angles of the nitrogen relative to the g tensor, θ_n, ϕ_n, therefore, are assumed to be 90°, 0° in sim-

ulations, to obtain the magnitude of superhyperfine tensors.

Deuterium Modulation. In the presence of many nuclei, the electron spin echo envelope modulation function V_{mod} is given by the product of the modulation functions due to each nucleus (Mims, 1972). In the presence of several different kinds of nuclei, the ESEEM function is thus given by the product of the modulation functions due to each kind of nucleus, e.g., protons, deuterons, and nitrogens:

$$V_{mod}(H,D,N) = V_{mod}(H)\, V_{mod}(D)\, V_{mod}(N)$$

By dividing the envelope modulation function obtained for a sample exchanged against D_2O with that of the same sample prepared in H_2O, we can eliminate modulations from nitrogen and from unexchanged protons in order to study the modulation effect of deuterium, so that

$$V_{mod}(D/H) = V_{mod}(D)/V_{mod}(H)$$

The modulations arising from deuterons are transformed into a positive peak at the low-frequency region of the ESEEM spectrum, while the modulations from protons give rise to a negative peak at the high-frequency region. These frequency differences are due to the difference in gyromagnetic ratio between deuterons and protons. Because the ESEEM spectrum of an enzyme in frozen solution is the average of modulations of many molecules with different orientations, the dividing procedure would completely eliminate the spectral contribution from nitrogen and unexchanged protons only if the average of the product is the same as the product of the average.

The deuterium modulation is attributed mainly to the electron–nuclear interaction, because the nuclear quadrupole interaction is so much smaller (Edmonds et al., 1976). At X-band, the deuterium Zeeman interaction is much larger than the isotropic component of the electron–nuclear coupling, so that the deuterium line in the ESEEM spectrum is centered about the deuterium Zeeman frequency and split slightly by the electron–nuclear coupling. However, in the cases of large anisotropy of the electron–nuclear interaction and the averaging effect of powder spectrum, the split line normally appears as a broadened line at the deuterium Zeeman frequency. This deuterium modulation can be examined in the ratioed data of both a two-pulse and a stimulated echo ESEEM spectrum. In a stimulated echo ESEEM, the deuterium modulation decays faster in the presence of a larger electron–nuclear interaction, leading to the broadening of the line at the deuterium Zeeman frequency in the Fourier transform. In the spectrum obtained from two-pulse ESEEM data, a stronger electron–nuclear interaction broadens the first harmonic of the deuterium modulation line, but has almost no effect on the second harmonic which arises from the combination of those two split lines (Dikanov et al., 1981; Shubin & Dikanov, 1983). Therefore, a stronger electron–nuclear coupling will result in a two-pulse echo with a faster decaying first harmonic and a more prominent second harmonic. In this way, two-pulse ESE is more sensitive than three-pulse ESE to the strength of the coupling between the Cu(II) unpaired electron and deuterons.

Results and Discussion

Cu(II)IPNS. The CW EPR spectrum of Cu(II)IPNS at pH 6.0 shows that at least 90% of the Cu(II) is in the same environment (Figure 1a). The spectrum was simulated with $g_{\parallel} = 2.346$, $A_{\parallel} = 465$ MHz, the approximately $g_{\perp} = 2.06$ and $A_{\perp} = 35$ MHz. Stimulated ESEEM data for Cu(II)IPNS together with its Fourier transform, recorded at 8.57 GHz and

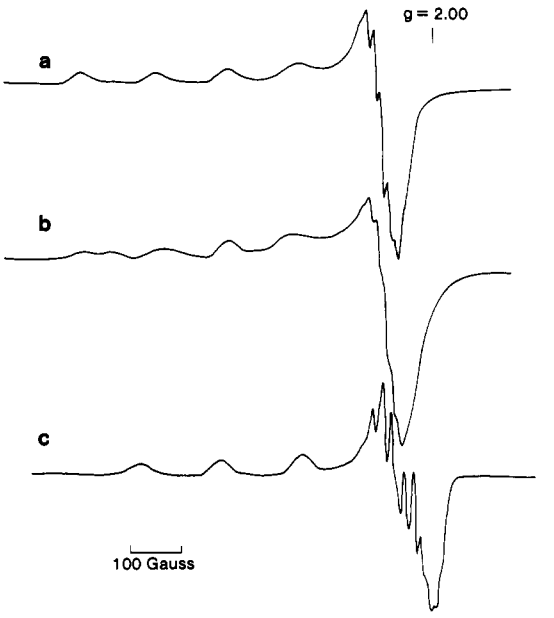

FIGURE 1: EPR spectra of Cu(II)IPNS at pH 6.0 (a) and at pH 7.1 (b), and of the Cu(II)IPNS–ACV complex at pH 7.1 (c). Measurement conditions: microwave frequency, 9.089 MHz; microwave power, 5 mW; modulation amplitude, 5.0 G; sample temperature, 77 K.

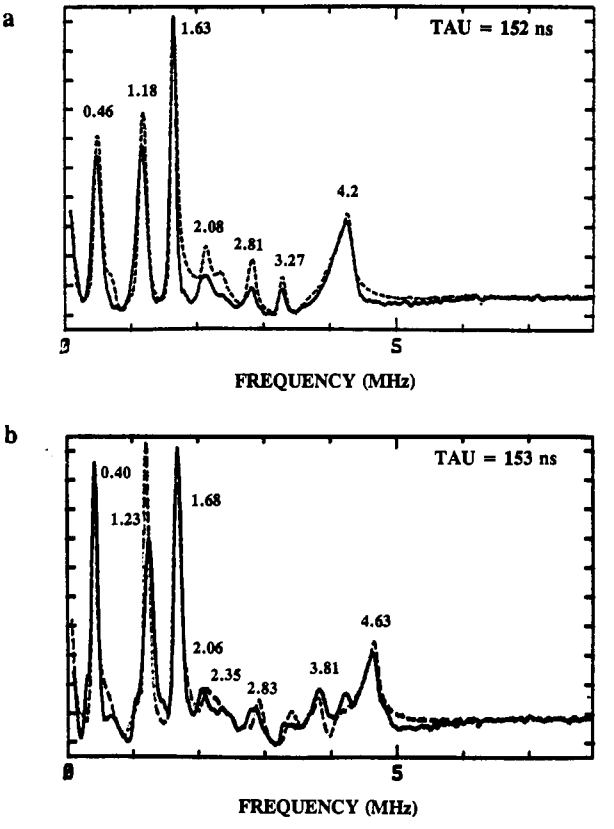

FIGURE 2: ESEEM spectra of Cu(II)IPNS in the absence (pH 6.0) (a) and presence (pH 7.1) (b) of the substrate ACV. Measurement conditions: (a) microwave frequency, 8.9262 GHz; magnetic field, 3088 G; microwave power, 56 W; sample temperature, 4.2 K; (b) microwave frequency, 8.8515 GHz; magnetic field, 3059 G; microwave power, 41 W; sample temperature, 4.2 K. Simulation parameters are given in Table I. Solid lines, experimental data; dashed lines, simulation.

at $g \doteq 2.07$, are shown in Figure 2a. Three sharp lines are obtained at 0.46, 1.18, and 1.63 MHz, and a double quantum line appears at about 4.15 MHz (less intense combination lines at intermediate frequencies are also seen, and they will be

Table I: Superhyperfine Coupling Parameters for Cu(II)IPNS and the Cu(II)IPNS–ACV Complex Obtained by ESEEM Spectral Simulations

	Cu(II)IPNS		Cu(II)IPNS–ACV	
ligand	N[a]	N[b]	N1[c]	N2
A_{iso} (MHz)	1.65	1.65	1.30	2.16
r_{eff} (Å)	3.00	2.80	3.25	3.10
θ, ϕ (deg)	90, 0	90, 0	90, 0	90, 0
e^2qQ (MHz)	1.85	1.79	1.78	1.90
η	0.50	0.54	0.68	0.43
α, β, γ	0, 0, 0	0, 0, 0	0, 0, 0	0, 0, 0

[a] The parameters obtained for both ^{14}N's in Cu(II)IPNS prepared at pH 6.0. [b] The parameters obtained for both ^{14}N's in Cu(II)IPNS prepared at pH 7.1. [c] N1 and N2 refer to the remote ^{14}N of the inequivalently coupled imidazoles in the Cu(II)IPNS–ACV complex.

discussed later). These four lines are characteristic of the interaction between the unpaired electron of Cu(II) and the remote nitrogen of the coordinated histidine imidazole under the condition of "exact cancellation". For Cu(II)IPNS, the two low-frequency NQI lines are well separated, as is found in some type 2 copper proteins (Kosman et al., 1980; McCracken et al., 1987, 1988a,b). This is different from the ESEEM spectra of type 1 copper proteins and the Cu(II)–DET–imidazole model compound where the two lowest frequency NQI lines collapse into one broad line (Mims & Peisach, 1978, 1979; McCracken et al., 1988a,b).

All ESEEM spectra for Cu(II)IPNS collected at several g values across the CW EPR spectrum have the same features. The frequencies of the NQI lines remain unchanged at different magnetic field settings, while the double quantum line frequency scales with magnetic field. Spectral simulations carried out at five different magnetic field settings yield values of 1.85 MHz and 0.50 for the nuclear quadrupole parameters e^2qQ and η, respectively, and values of 1.65 MHz and 3.00 Å for the electron–nuclear coupling constant A_{iso} and the effective distance r_{eff} (Table I).

Besides the four characteristic lines of the superhyperfine interaction between the Cu(II) unpaired electron and ^{14}N of imidazole, there are also three minor lines at 2.08, 2.81, and 3.27 MHz (Figure 2a). These are combinations of the three NQI lines, and they are expected to appear when more than one imidazole is bound to Cu(II) (Mims, 1972). Simulations of ESEEM and spectra for Cu(II)IPNS at $g = 2.07$ and $\nu = 8.57$ GHz, for one-, two- and three-nitrogen cases, together with the experimental result, are shown in Figure 3. In the echo decay data for more than a single nitrogen (Figure 3a,b), there are extra high-frequency components around the $\tau + T = 0.1$ μs region of the decay envelope. Fourier transform shows that the intensities of the combination lines are proportional to the number of interacting ^{14}N nuclei (Figure 3e–g). From a comparison with the experimental results (Figure 3d,h), it is suggested that there are at least two equatorially bound histidine nitrogens contributing to the ESEEM.

However, the intensities of combination lines in the simulated spectrum for two nitrogen are a little greater than for the experimental results. A possible explanation is that both nitrogens may not have the same magnetic coupling. A difference in the strength of coupling, that is, the isotropic component of the electron–nuclear interaction A_{iso}, would result in a difference in their individual contributions to the intensities of the NQI lines. Their combination would then be less intense than that for two equivalent nitrogens. When two nitrogens with slightly different values of A_{iso} were used to simulate the spectrum, the fitting for the intensity of the combination lines

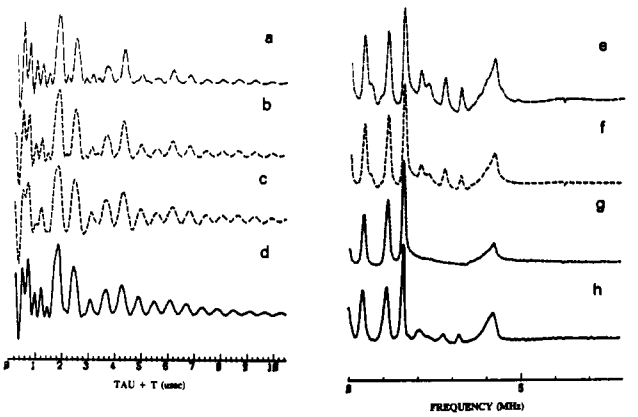

FIGURE 3: Simulation of ESEEM data and Fourier transforms for one (c, g), two (b, f), and three (a, e) imidazole nitrogens interacting with Cu(II), together with experimental data (d, h) for Cu(II)IPNS. Measurement conditions: same as in Figure 2a. Simulation parameters: $A_{iso} = 1.65$ MHz, $r_{eff} = 3.00$ Å, $e^2qQ = 1.85$ MHz, $\eta = 0.50$, $\tau = 152$ ns; microwave frequency, 8.9262 GHz; magnetic field, 3088 G.

is improved. When these values were set more than 0.15 MHz apart, the double quantum line splits in the simulation, and this is not seen in the data. Therefore, the difference in A_{iso} cannot exceed 0.15 MHz.

Not only does the strength of the magnetic coupling have an effect on the relative intensities of the combination lines, a difference in the orientation of the two imidazole planes, which determines the orientation of the principal axis of the efg tensor relative to those of the g tensor, would also result in a difference. Due to the complications of the powder average effect in a frozen solution measurement, the difference in the orientation of two imidazole planes and the difference in the coupling constant of two nitrogens cannot be accurately determined and are thus assumed to be the same in the spectral simulation.

When the pH of the sample is raised to 7.1, another Cu(II) site with $g_{\parallel} = 2.320$ and $A_{\parallel} = 370$ MHz, and approximately $g_{\perp} = 2.05$ and $A_{\perp} = 35$ MHz, appears in the CW EPR spectrum (Figure 1b; Ming et al., 1990). The ESEEM of this sample is almost the same as that of Cu(II)IPNS at pH 6.0, with slightly greater line width and a slight shift of NQI frequencies. In the spectrum recorded at 8.87 GHz and 3066 G, three sharp lines are seen at 0.48, 1.14, and 1.63 MHz, and the double quantum line is at 4.21 MHz (data not shown). The line broadening and slight shift of ESE resonances suggest that the imidazole nitrogens in the high-pH Cu(II) site might have a slightly different coupling from those in the low-pH Cu(II) site. With the assumption of the same anisotropy in the electron–nuclear interaction, the values 1.79 MHz and 0.54 are obtained for the nuclear quadrupole parameters e^2qQ and η, respectively, to give the shifted NQI lines in a spectral simulation assuming equal population of each type of Cu(II) site. The isotropic part of the electron–nuclear interaction, A_{iso}, of the high-pH Cu(II) site has to be slightly different from that of the low-pH site to give the broadened NQI and double quantum lines. Were the difference in A_{iso} to be more than 0.15 MHz, a splitting would be seen in the double quantum line obtained in the simulation. As no splitting is seen, the difference cannot be larger than 0.15 MHz.

Even though the CW EPR spectrum shows that there are two inequivalent Cu(II) binding sites in Cu(II)IPNS at pH 7.1, very little difference in the ^{14}N superhyperfine interaction between the Cu(II) unpaired electron with histidine imidazole is observed for the individual Cu(II) binding sites. This

suggests that the local environment and the strength of magnetic coupling arising from coordinated histidine nitrogen is similar in both types of copper sites. Therefore, if the histidine ligand composition is the same for both Cu(II) sites, the difference between the two inequivalent binding sites in Cu(II)IPNS as determined by CW EPR probably arises from a difference in other ligands, e.g., a difference in the protonation state of a bound water molecule.

Cu(II)IPNS–ACV Complex. ACV binds to Cu(II)IPNS at pH 7.1 to form a complex that shows an intense S-to-Cu charge-transfer band at 385 nm (Ming et al., 1990). Titration of Cu(II)IPNS with ACV monitored by the 385-nm band exhibits a linear relationship of $(A - A_0)$ vs [ACV] which levels off at [Cu(II)IPNS] = [ACV], suggesting the formation of a 1:1 Cu(II)IPNS–ACV complex with the substrate tightly bound to the Cu(II). The CW EPR spectrum of the Cu(II)IPNS–ACV complex (Figure 1c) is that of a single paramagnetic species whose spectrum can be simulated with the parameters $g_\parallel = 2.234$, $g_\perp = 2.04$, $A_\parallel = 498$ MHz, and $A_\perp = 54$ MHz.

At $g = 2.068$ and 8.85 GHz, near $g_\perp$, the ESEEM spectrum of Cu(II)IPNS with substrate is more complicated than the spectrum of Cu(II)IPNS alone, as shown in Figure 1b. Three sharp NQI lines are obtained at 0.40, 1.23, and 1.68 MHz, shifted from those for Cu(II)IPNS in the absence of substrate. The broad double quantum line is now at 4.63 MHz, different by 0.4 MHz from that seen before. Also there is a new line at 3.81 MHz, 0.8 MHz lower than for the double quantum line. This line is so far removed from the double quantum line that it is likely not due to the anisotropy of the electron–nuclear interaction at the same transition. It has similar line shape as the double quantum line, although its shoulder is very close to one of the combination lines in the spectrum so that it cannot be clearly resolved when studied at $g = 2.068$ (Figure 4c).

When the spectrum was recorded at 10.8 GHz and the same g value, this line scales up with the double quantum line and assumes the same line shape, with a resolved shoulder at the low-frequency end, without the interference of the combination lines (Figure 4a). When the spectrum was recorded at lower magnetic fields within the EPR line, the 3.81-MHz line scales down together with the double quantum line and both have the same shape. At $g = 2.175$ (Figure 4b), it splits into two lines, at 3.46 and 3.69 MHz, analogous to the double quantum line which also splits into two features at 4.17 and 4.41 MHz.

The 3.81-MHz line does not arise from the combination of the double quantum line (4.63 MHz) with lower frequency NQI lines in the spectrum. No combination of the double quantum line with any primary NQI lines would yield a frequency of 3.81 MHz. Also the combination of the double quantum line with a resultant line arising from more than one NQI lines would have much weaker intensity than that of the 3.81-MHz line. Therefore, the 3.8-MHz line observed at 8.8 GHz must arise from a double quantum transition of a second ^{14}N which is more weakly coupled than the first. By spectral simulation, values of 1.30 and 2.16 MHz were obtained for the superhyperfine coupling constants, A_{iso} for the two nitrogens.

In Figure 2b, we show that the combination lines at 2.06, 2.35, 2.83, and 3.3 MHz for Cu(II)IPNS in the presence of ACV to be very weak and relatively broad. The troughs in the spectrum suggest that they arise from combination lines of slightly different primary lines. Because the more strongly coupled ^{14}N satisfies the "exact cancellation" condition better than does the weaker one, the primary lines associated with it would be much more intense than those from the weakly

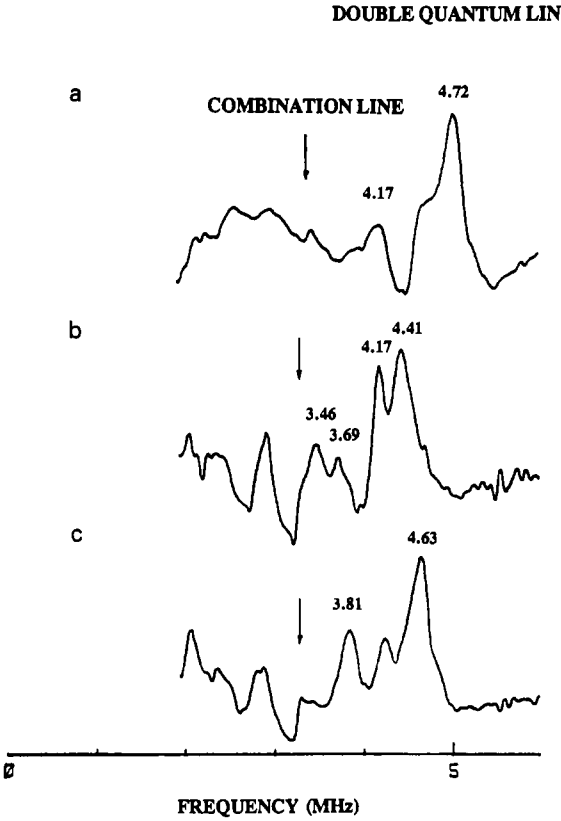

FIGURE 4: Double quantum lines of Cu(II)IPNS–ACV. The ESEEM spectra were recorded at (a) 8.8514 GHz and 3059 G, (b) 8.8514 GHz and 2908 G, and (c) 10.8305 GHz and 3742 G. The arrow indicates one of the combinations of the NQI lines.

coupled ^{14}N. Even if the two sets of primary lines were slightly different from each other, the strong one would overshadow the weaker ones so that the NQI lines of the weakly coupled nitrogen would not be as well resolved.

The differences in the NQI lines of these two nitrogens are better observed in the spectrum obtained at a longer value of τ. With $\tau = 230$ ns, the 1.23-MHz line seen at the shorter τ value splits into two lines, at 1.07 and 1.23 MHz (data not shown). The same phenomenon is observed in spectra taken with other longer τ values at other g values (Figure 7d). The 1.07-MHz line, therefore, must be the second NQI line from the more weakly coupled nitrogen. If we assume that the 0.6-MHz line, which appears as a shoulder on the 0.4-MHz line, is the first NQI line of the weakly coupled nitrogen, and 1.68 MHz is the third, then 1.78 MHz and 0.68 are obtained by simulation for the nuclear quadrupole constants e^2qQ and η, respectively, for this weakly coupled nitrogen. Assuming that 0.40, 1.23, and 1.68 MHz are the three NQI lines of the strongly coupled nitrogen, the values of 1.90 MHz and 0.43 for e^2qQ and η are more accurately obtained in the spectral simulation, since all three NQI lines are very well resolved.

A spectral simulation for two nitrogens, each with different NQI and superhyperfine couplings, is shown in Figure 5c,g. We also show two other simulations, one with two strongly coupled nitrogens and one weakly coupled nitrogen (Figure 5a,e), and the other with one strongly coupled nitrogen and two weakly coupled nitrogens (Figure 5b,f). The simulation with two nitrogens having different A_{iso} values gives the best fit on the basis of both the relative amplitude of the double quantum lines and the amplitude of the combination lines. This suggests that the Cu(II)IPNS–ACV complex has two inequivalent equatorially bound histidine ligands, with one

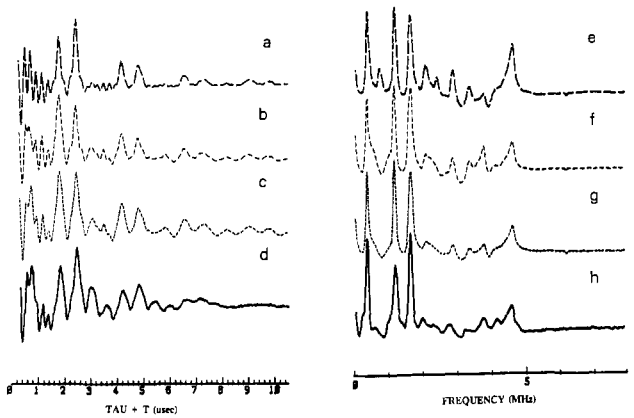

FIGURE 5: Simulation of ESEEM data and Fourier transforms for one strongly coupled and one weakly coupled (c, g), one strongly coupled and two weakly coupled (b, f), and two strongly coupled and one weakly coupled (a, e) nitrogens interacting with Cu(II), together with experimental data (d, h) for Cu(II)IPNS–ACV. Measurement conditions: same as in Figure 2b. Simulation parameters: weakly coupled nitrogen N1, A_{iso} = 1.30 MHz, r_{eff} = 3.25 Å, e^2qQ = 1.78 MHz, η = 0.68; strongly coupled nitrogen N2, A_{iso} = 2.16 MHz, r_{eff} = 3.10 Å, e^2qQ = 1.90 MHz, η = 0.43, τ = 153 ns; microwave frequency, 8.8514 GHz; magnetic field, 3059 G.

nitrogen coupled to the Cu(II) unpaired electron almost twice as strongly as the other.

Effect of ACV. The binding of ACV removes the ligand inhomogeneity of the Cu(II) site seen at pH 7.1 and changes the ligand geometry at the Cu(II) site (Figure 1). Without ACV, two nearly equivalent histidine ligands are coupled to Cu(II), on the basis of the similar superhyperfine couplings obtained for both nitrogens. In the presence of ACV, the Cu(II) unpaired electron delocalizes differently onto the two histidine ligands, more to one histidine ligand to make its coordination more covalent and less to the other to give a 0.86-MHz difference in the isotropic component of the superhyperfine interaction (Table I). This difference of the delocalization of the unpaired electron to two histidine imidazole ligands can arise from a change of geometry at the Cu(II) site through a structural change and/or a rearrangement of the orbital directions. The binding of ACV may move one histidine ligand away from the equatorial plane toward a more axial position, where the delocalization of the $d_{x^2-y^2}$ ground-state unpaired electron is less favorable. Moving a ligand to a more axial position lengthens the Cu–N bond, thereby weakening the coupling. The other histidine ligand may move closer to the equatorial plane to give a stronger coupling.

Number of Histidine Ligands. Simulations of ESEEM for Cu(II)IPNS both in the presence and in the absence of ACV show that two histidine nitrogens give spectra close to the experimental results. At X-band, for a $d_{x^2-y^2}$ ground-state Cu(II), only the remote nitrogen of equatorially bound histidine imidazole has an electron–nuclear interaction close to the nuclear Zeeman interaction to satisfy the "exact cancellation" condition so as to produce deep modulations. Axially bound histidine imidazole nitrogen interacts with Cu(II) much more weakly so that the modulation from it is very shallow (Cornelius et al., 1990). In the presence of two nearly equatorial histidine ligands, the contribution from an axial histidine ligand will not likely be observed. Therefore, our ESEEM results cannot rule out the possibility of the presence of an additional histidine ligand bound axially. NMR results for Fe(II)IPNS and Co(II)IPNS suggest that there are a total of three endogenous histidine ligands bound to the metal (Ming et al., 1990). If the same structure is maintained

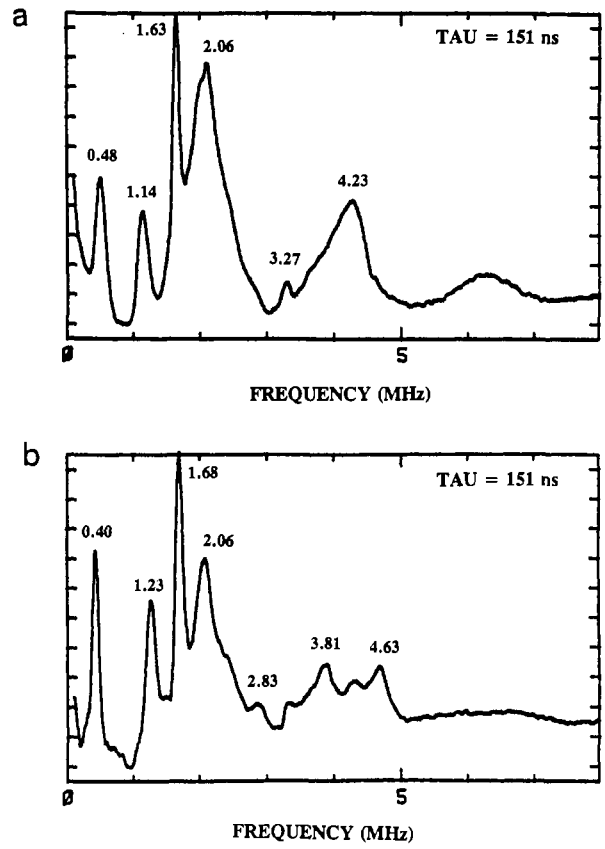

FIGURE 6: ESEEM data and Fourier transform of Cu(II)IPNS in the absence (a) and presence (b) of ACV in D_2O. The 2.06 MHz line in both traces arises from deuterium modulations. Measurement conditions: (a) microwave frequency, 9.0172 GHz; magnetic field, 3118 G; microwave power, 35 W; temperature, 4.2 K; (b) microwave frequency, 9.0247 GHz; magnetic field, 3118 G; microwave power, 33 W; temperature, 4.2 K.

for Cu(II)IPNS, two of them are nearly equatorially coordinated to the metal and the third, if present, must be axially bound.

Hydrogen Bonding to the Remote Nitrogen of Histidine Ligand. The NQI lines of both Cu(II)IPNS and the Cu(II)IPNS–ACV complex are similar to those found for type 2 Cu(II) proteins. An early ESEEM study of Cu(II)-coordinated substituted imidazole model compounds had shown that the NQI parameters are related to the polarization of the N–H bond (Jiang et al., 1990). The remote N–H bond of Cu(II)-coordinated imidazole having NQI parameters similar to those for type 2 copper proteins is much less polarized than where the remote nitrogen is hydrogen bonded. Therefore, the remote nitrogens of Cu(II)-coordinated histidine ligands in IPNS are probably weakly hydrogen bonded. The asymmetry parameter η is lower and the quadrupole coupling constant e^2qQ is higher for the more strongly coupled histidine nitrogen in the presence of substrate. This suggests that the N–H bond at this remote nitrogen is less polarized in the presence of ACV than in its absence.

Cu(II)IPNS in D_2O. The possibility of water coordination to the metal site in Cu(II)IPNS and Cu(II)IPNS–ACV was examined by studying the ESEEM of the enzyme exchanged in D_2O buffer. The stimulated echo ESEEM data for Cu(II)IPNS in D_2O (pD 7.1) is shown in Figure 6a. The four characteristic lines from histidine nitrogens are the same as for Cu(II)IPNS in H_2O at pH 7.1, showing that the nitrogen nuclear quadrupole interaction and the electron–nuclear hyperfine interactions are not changed in D_2O buffer. An extra line at about 2.07 MHz, near the deuterium Zeeman frequency

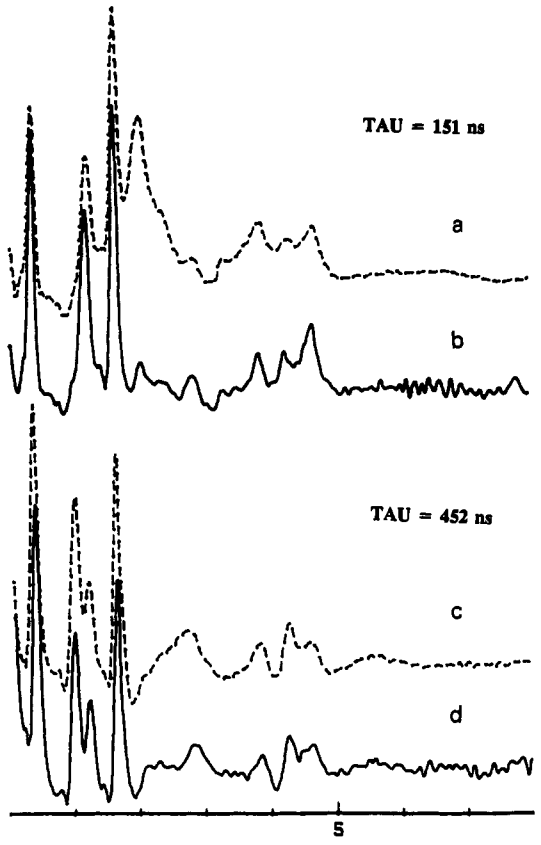

FIGURE 7: Comparison of ESEEM spectra of Cu(II)IPNS + ACV in D_2O (a, c) and H_2O (b, d) at different τ values. At τ = 151 ns, the presence of deuterium modulation increases the intensity of the double quantum line at 3.81 MHz, while at τ = 452 ns, the deuterium modulation is suppressed and no difference is observed in the intensity of the double quantum lines for the samples in D_2O and H_2O.

of 2.04 MHz at the measuring magnetic field of 3118 G, is seen in the spectrum. The frequency of this line scales with the deuterium Zeeman frequency in spectra obtained at other magnetic fields and is believed to arise from deuterium interaction. The broad deuterium line is split about 0.1 MHz, suggesting that there is strong dipolar or contact coupling between the unpaired electron and deuterons. Therefore, there must be deuterons in close proximity to the Cu(II) site.

Cu(II)IPNS–ACV in D_2O. The CW EPR spectrum of Cu(II)IPNS–ACV is the same in D_2O and H_2O. In the stimulated ESEEM spectrum shown in Figure 6b, there is also a deuterium line at 2.06 MHz, but with less intensity and narrower line width, compared to the deuterium line in the spectrum of Cu(II)IPNS in D_2O buffer (Figure 6a). This suggests that there are less deuterons accessible to the Cu(II) site when ACV is present, even though water still remains as a metal ligand (see below). The same nitrogen modulations attributed to two inequivalent couplings are also seen here. Contrary to what was observed in the sample prepared in H_2O, where the intensity of the double quantum line (3.85 MHz) of weakly coupled nitrogen is almost half of that (4.65 MHz) of the strongly coupled nitrogen (Figure 7b), the intensity of the double quantum line of the weakly coupled nitrogen here is almost the same as that of the strongly coupled nitrogen (Figure 7a). Because the intensity of the double quantum line is proportional to the number of the nitrogen nuclei equatorially bound to Cu(II), and the simulation for two weakly coupled nitrogens and one strongly coupled nitrogen has two double quantum lines of similar intensities (Figure 5f), this raises a question concerning the assignment made above for

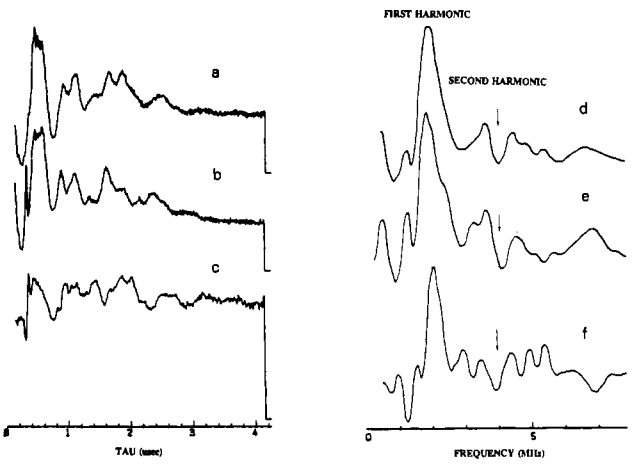

FIGURE 8: Deuterium modulation data (obtained by the ratio method described in the text) and Fourier transforms for Cu(II)IPNS (a, d) and for Cu(II)IPNS–ACV (b, e). Trace c is the result of dividing (a) by (b), and (f) is the Fourier transform. The arrows indicate the negative second harmonic of the deuterium Zeeman frequency.

the number of equatorially bound histidine nitrogens. However, the combination of one of the nitrogen NQI lines at 1.68 MHz with the 2.07-MHz deuterium line could give a line at 3.75 MHz, close to the frequency of the double quantum line of the weakly coupled nitrogen. Therefore, the increase of the intensity of the 3.85 MHz line might be a consequence of deuterium interaction.

This is demonstrated from the spectra studied at long τ values, where the multiple of the periodicity arising from the proton happens to be close to the multiple of the periodicity arising from deuterons. The modulations arising from the deuterium interaction, therefore, are also largely suppressed. At τ = 452 ns, the broad deuterium line at 2.07 MHz can no longer be seen, and we would not expect to see the effect of deuterium modulation on the double quantum lines. Figure 7c,d shows that the relative intensities of two double quantum lines are the same in the spectra of Cu(II)IPNS–ACV complex in D_2O and in H_2O at this τ value, where both deuterium and proton contributions are suppressed. The same results are also seen in spectra obtained at other g values. Therefore, the apparent increase of the intensity of the double quantum line of weakly coupled nitrogen is due to deuterium interaction. The conclusion that there are two equatorially bound histidine ligands remains valid.

Water Coordination. The appearance of deuterium modulations in stimulated echo ESEEM suggests that the Cu(II) site of IPNS is readily accessible to the solvent. The two-pulse spin echo was used to extract the deuterium modulations and to assess the strength of the coupling between the unpaired electron and deuterons. For Cu(II)IPNS in D_2O, the two-pulse ESEEM collected at 4.2 K decays very fast so that it damps to the base line in about 1.2 μs. The ratio of two ESE collected for Cu(II)IPNS in D_2O and H_2O only shows two cycles of deuterium modulations. In order to increase the phase memory, the temperature was lowered to 1.8 K, which increases the two-pulse ESE modulation beyond 2.6 μs. Figure 8a shows the ratio of the two-pulse ESEEM for Cu(II)IPNS in D_2O with that in H_2O. The ratio of ESE envelopes for Cu(II)IPNS–ACV in D_2O with that in H_2O is different from that for Cu(II)IPNS alone, as shown in Figure 8b. In the presence of substrate, the modulation depth of the first harmonics is shallower and that of the deuterium second harmonic is relatively stronger (compare Figure 8d with Figure 8e).

Early model studies on the deuterium modulation of Cu(II)–mono-, –bis-, and –trisbipyridyl model compounds

(McCracken et al., 1987) showed that the deuterons on water molecules that are not coordinated to Cu(II) give an ESEEM with a periodicity of about 500 ns, corresponding to the deuterium nuclear Zeeman frequency of about 2 MHz at 3 kG. The deuterons on an axially bound water give a stronger ESE modulation, which yields both the first harmonic and second harmonic of the deuterium nuclear Zeeman frequency. The modulation from deuterons on equatorially bound water emphasizes the first harmonic of the deuterium nuclear Zeeman interaction, but it decays faster and, more important, the second harmonic appears much more pronounced than that for deuterons on an axial ligand.

The presence of a strong second harmonic of the deuterium Zeeman frequency of two-pulse ESEEM spectra for Cu(II)-IPNS and the splitting of the deuterium peak in the stimulated echo ESEEM spectrum suggest that deuterons are strongly coupled to Cu(II). Comparison between the deuterium modulation obtained for Cu(II)IPNS and Cu(II)IPNS–ACV with that of model compounds suggests that the protein shows a deuterium modulation comparable to that for deuterium on an equatorially coordinated water. However, the deuterium modulation pattern in the model compounds shows only two periodicities corresponding to first and second harmonics of deuterium Zeeman frequency, while another low-frequency modulation can also be observed in the protein spectrum. The ratio of the intensity of second harmonic to that of the first harmonic is much greater in Cu(II)IPNS both in the absence and in the presence of ACV than in models, which suggests that the coupling of the Cu(II) unpaired electron with deuterons is stronger than that in the model compounds studied. This coupling is so much stronger that the splitting of the deuterium lines is resolved (about 0.1 MHz) and the difference of two split deuterium lines is large enough to give an observable negative low-frequency peak in the Fourier transform near 0.8 MHz [see Shubin and Dikanov (1983) eq 10].

The ratio of deuterium modulation for Cu(II)IPNS with that for Cu(II)IPNS–ACV was used to examine the deuterons that are replaced by ACV (Figure 8c). Fourier transform shows a strong first harmonic of the deuterium Zeeman frequency and a minor second harmonic, as well as some other components (Figure 8f). This suggests that the binding of ACV to the Cu(II) site displaces a coordinated water molecule. Because of the noise introduced by the double ratioing of ESEEM data, it cannot be unequivocally determined whether the coordinated water molecule is equatorially or axially bound.

Concluding Remarks. In this report we have presented evidence for the presence of two equatorially coordinated His residues (A_{iso} = 1.65 MHz for the remote nitrogen) in the metal site of IPNS by ESEEM studies. ACV binding to Cu(II)IPNS causes a significant perturbation of the magnetic coupling of the coordinated His residues with the Cu(II) center so that A_{iso} of the remote nitrogen becomes 1.30 MHz for one His and 2.16 MHz for the other. The ESEEM studies also suggest that water, as a ligand of the Cu(II) in IPNS, is displaced upon ACV binding.

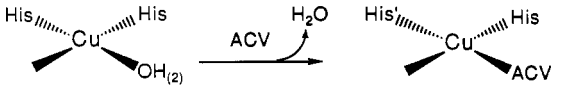

Although CW EPR shows two inequivalent Cu(II) sites in IPNS at pH 7.1, the two types of Cu(II) sites seem to have almost identical endogenous environments from the ESEEM studies, suggesting that the origin of the heterogeneity is due to an acid–base equilibrium of a coordinated water molecule with relatively low pK_a value. The presence of a coordinated OH^- in the metal site of IPNS might be important for the enzyme–substrate interaction.

References

Baldwin, J. E. (1989) in *Recent Advances in the Chemistry of β-Lactam Antibiotics* (Bentley, P. J., & Southgate, R., Eds.) Chapter 1, Royal Society of Chemistry, London.

Baldwin, J. E., & Abraham, E. (1988) *Nat. Prod. Rep. 5*, 129–145.

Baldwin, J. E., & Bradley, M. (1990) *Chem. Rev. 90*, 1079–1088.

Belford, R. L., & Nilges, M. J. (1979) International Electron Paramagnetic Resonance Symposium, 21st Rocky Mountain Conference, Denver, CO.

Britt, R. D., & Klein, M. P. (1987) *J. Magn. Reson. 74*, 535–540.

Chen, V. J., Orville, A. M., Harpel, M. R., Frolik, C. A., Surerus, K. K., Münck, E., & Lipscomb, J. D. (1989) *J. Biol. Chem. 264*, 21677–21681.

Cornelius, J. B., McCracken, J., Clarkson, R., Belford, R. L., & Peisach, J. (1990) *J. Phys. Chem. 94*, 6977–6982.

Dikanov, S. A., Shubin, A. A., & Parmon, V. N. (1981) *J. Magn. Reson. 42*, 474–487.

Edmonds, D. T., Goren, S. D., Mackay, A. L., White, A. A. L., & Sherman, W. F. (1976) *J. Magn. Reson. 23*, 505–514.

Flanagan, K. L., & Singel, D. J. (1987) *J. Chem. Phys. 87*, 5606–5616.

Henderson, T. A., Hurst, G. C., & Kreilick, R. W. (1985) *J. Am. Chem. Soc. 107*, 7299–7303.

Hurst, G. C., Henderson, T. A., & Kreilick, R. W. (1985) *J. Am. Chem. Soc. 107*, 7294–7299.

Jiang, F., McCracken, J., & Peisach, J. (1990) *J. Am. Chem. Soc. 112*, 9035–9044.

Kevan, L. (1979) *Time Domain Electron Spin Resonance* (Kevan, L., & Schwartz, R. N., Eds.) pp 279–342, Wiley-Interscience, New York.

Kosman, D. J., Peisach, J., & Mims, W. B. (1980) *Biochemistry 19*, 1304–1308.

Kriauciunas, A., Frolik, C. A., Hassell, T. C., Skatrud, P. L., Johnson, M. G., Holbrook, N. L., & Chen, V. J. (1991) *J. Biol. Chem. 266*, 11779–11788.

Lin, C. P., Bowman, M. K., & Norris, J. R. (1985) *J. Magn. Reson. 65*, 369–374.

Maurice, A. M. (1981) Ph.D Thesis, University of Illinois, Urbana, IL.

McCracken, J., Peisach, J., & Dooley, D. M. (1987) *J. Am. Chem. Soc. 109*, 4064–4072.

McCracken, J., Pember, S., Benkovic, S. J., Villafranca, J. J., Miller, R. J., & Peisach, J. (1988a) *J. Am. Chem. Soc. 110*, 1069–1074.

McCracken, J., Desai, P. R., Papadopoulos, N. J., Villafranca, J. J., & Peisach, J. (1988b) *Biochemistry 27*, 4133–4137.

McCracken, J., Cornelius, J. B., & Peisach, J. (1989) *Pulsed EPR: A New Field of Applications* (Keijzers, C. P., Reijerse, E. J., & Schmidt, J., Eds.) pp 156–161, North-Holland Publishing, Co., Amsterdam.

Mims, W. B. (1972) *Phys. Rev. 5*, 2409–2419.

Mims, W. B. (1984) *J. Magn. Reson. 59*, 291–306.

Mims, W. B., & Peisach, J. (1978) *J. Chem. Phys. 19*, 4921–4930.

Mims, W. B., & Peisach, J. (1979) *J. Biol. Chem. 254*, 4321–4323.

Mims, W. B., & Peisach, J. (1981) in *Biological Magnetic Resonance* (Berliner, L. J., & Reuben, J., Eds.) Vol. 3, pp 213-263, Plenum, New York.
Mims, W. B., Davis, J. L., & Peisach, J. (1984) *Biophys. J. 45*, 755-766.
Ming, L.-J., Que, L., Jr., Kriauciunas, A., Frolik, C. A., & Chen, V. J. (1990) *Inorg. Chem. 29*, 1111-1112.
Nilges, M. J. (1979) Ph.D. Thesis, University of Illinois, Urbana, IL.
Robinson, J. A. (1988) *Chem. Soc. Rev. 17*, 383-452.
Shubin, A. A., & Dikanov, S. A. (1983) *J. Magn. Reson. 52*, 1-12.
Zweier, J. L., Peisach, J., & Mims, W. B. (1982) *J. Biol. Chem. 257*, 10314-10316.

Electrochemical and Kinetic Analysis of Electron-Transfer Reactions of *Chlorella* Nitrate Reductase†

Christopher J. Kay,‡ Larry P. Solomonson, and Michael J. Barber*
Department of Biochemistry and Molecular Biology, University of South Florida, College of Medicine, Tampa, Florida 33612
Received June 25, 1991; Revised Manuscript Received September 11, 1991

ABSTRACT: Assimilatory nitrate reductase (NR) from *Chlorella* is homotetrameric, each subunit containing FAD, heme, and Mo-pterin in a 1:1:1 stoichiometry. Measurements of NR activity and steady-state reduction of the heme component under conditions of NADH limitation or competitive inhibition by nitrite suggested intramolecular electron transfer between heme and Mo-pterin was a rate-limiting step and provided evidence that heme is an obligate intermediate in the transfer of electrons between FAD and Mo-pterin. In addition to the physiological substrates NADH and nitrate, various redox mediators undergo reactions with one or more of the prosthetic groups. These reactions are coupled by NR to NADH oxidation or nitrate reduction. To test whether intramolecular redox reactions of NR were rate-determining, rate constants for redox reactions between NR and several chemically diverse mediators were measured by cyclic voltammetry in the presence of NADH or nitrate. Reduction of ferrocenecarboxylic acid, dichlorophenolindophenol, and cytochrome *c* by NADH-reduced NR was coupled to reoxidation at a glassy carbon electrode (ferrocene and dichlorophenolindophenol) or at a bis(4-pyridyl) disulfide modified gold electrode (cytochrome *c*), yielding rate constants of 10.5×10^6, 1.7×10^6, and 2.7×10^6 M^{-1} s^{-1}, respectively, at pH 7. Kinetics were consistent with a second-order reaction, implying that intramolecular heme reduction by NADH and endogenous FAD was not limiting. In contrast, reduction of methyl viologen and diquat at a glassy carbon electrode, coupled to oxidation by NR and nitrate, yielded similar kinetics for the two dyes. In both cases, second-order kinetics were not obeyed, and reoxidation of dye-reduced Mo-pterin of NR by nitrate became limiting at low scan rates. Minimum estimates for NR reduction of 4.3×10^6 M^{-1} s^{-1} were obtained by extrapolation to infinite scan rate. These results suggest that reoxidation of reduced Mo-pterin by nitrate is rate-limiting for these partial activities of NR.

Intramolecular electron transfers between the prosthetic groups of assimilatory nitrate reductase (NR)[1] from *Chlorella* serve to conduct reducing equivalents from FAD, the site of NADH oxidation (Solomonson & Barber, 1990), via heme to the Mo-pterin[2] center, where nitrate is reduced to nitrite. The oxidation-reduction midpoint potentials of the three centers are consistent with essentially irreversible electron-transfer reactions in the physiological direction (Kay et al., 1988) since the electron affinities of the centers are well separated. In addition to NADH-dependent nitrate reduction, cytochrome *c* and a number of low molecular weight mediators can undergo redox reactions with one or more of the prosthetic groups. The partial activities which result from these reactions fall into two categories: NADH dehydrogenase activities, in which NADH-reduced NR may reduce cytochrome *c* (NADH:CR), DCPIP (NADH:DR), or ferricyanide (NADH:FR), and nitrate-reducing activities, in which reduced exogenous flavin (FH_2:NR), bromophenol blue (BPB:NR), or MV radical cation (MV:NR) act as electron donors (Solomonson & Barber, 1990). The relative rates of the partial activities indicate that NADH dehydrogenase activities are several times faster than the nitrate-reducing activities. Further evidence that rate limitation is associated with nitrate reduction was obtained from the observation that the heme is >80% reduced under conditions of optimal turnover (Kay & Barber, 1986). In the present study, we have investigated whether the NADH dehydrogenase and nitrate-reducing

† This work was supported by the National Institutes of Health (1 RO1 GM32696) and the United States Department of Agriculture (CSRS 88-37120-3871).
* Address correspondence to this author at the Department of Biochemistry and Molecular Biology, University of South Florida, College of Medicine, MDC Box 7, Tampa, FL 33612.
‡ Present address: Biosciences Division, General Atomics, P.O. Box 85608, San Diego, CA 92186-9784.

[1] Abbreviations: DCPIP, 2,6-dichlorophenolindophenol; DQ, diquat (6,7-dihydrodipyrido[1,2-*a*:2',1'-*c*]pyrazinediium); EDTA, ethylenediaminetetraacetic acid; FRC, ferrocenecarboxylic acid; G6P, D-glucose 6-phosphate; G6PDH, NADH:D-glucose dehydrogenase (EC 1.1.1.49); MOPS, 3-(*N*-morpholino)propanesulfonic acid; MV, methyl viologen (1,1'-dimethyl-4,4'-bipyridinium dichloride); MV:NR, reduced methyl viologen:nitrate reductase; NADH:CR, NADH:cytochrome *c* reductase; NADH:FRCR, NADH:ferrocenecarboxylic acid reductase; NR, nitrate reductase; LSV, linear sweep voltammetry; NHE, normal hydrogen electrode; GCE, glassy carbon electrode.
[2] The term "Mo-pterin" refers to the complex of Mo, molybdopterin, and associated protein ligands to Mo.

0006-2960/91/0430-11445$02.50/0